Dynamics of Urokinase Receptor Interaction with Peptide Antagonists Studied by Amide Hydrogen Exchange and Mass Spectrometry†

Thomas J. D. Jørgensen,*,‡,§ Henrik Gårdsvoll,§ Keld Danø,§ Peter Roepstorff,‡ and Michael Ploug§

Department of Biochemistry and Molecular Biology, University of Southern Denmark, Campusvej 55, DK-5230 Odense M, Denmark, and Finsen Laboratory, Rigshospitalet, Strandboulevarden 49, DK-2100 Copenhagen Ø, Denmark

Received June 22, 2004; Revised Manuscript Received September 15, 2004

ABSTRACT: Using amide hydrogen exchange combined with electrospray ionization mass spectrometry, we have in this study determined the number of amide hydrogens on several peptides that become solvent-inaccessible as a result of their high-affinity interaction with the urokinase-type plasminogen activator receptor (uPAR). These experiments reveal that at least six out of eight amide hydrogens in a synthetic nine-mer peptide antagonist (AE105) become sequestered upon engagement in uPAR binding. Various uPAR mutants with decreased affinity for this peptide antagonist gave similar results, thereby indicating that deletion of the favorable interactions involving the side chains of these residues in uPAR does not affect the number of hydrogen bonds established by the main chain of the peptide ligand. The isolated growth factor-like domain (GFD) of the cognate serine protease ligand for uPAR showed 11 protected amide hydrogens in the receptor complex. Interestingly, a naturally occurring O-linked fucose on Thr^{18} confers protection of two additional amide hydrogens in GFD when it forms a complex with uPAR. Dissociation of the uPAR−peptide complexes is accompanied by a correlated exchange of nearly all amide hydrogens on the peptide ligand. This yields bimodal isotope patterns from which dissociation rate constants can be determined. In addition, the distinct bimodal isotope distributions also allow investigation of the exchange kinetics of receptor-bound peptides providing information about the local structural motions at the interface. These exchange experiments therefore provide both structural and kinetic information on the interaction between uPAR and these small peptide antagonists, which in model systems show promise as inhibitors of intravasation of human cancer cells.

Identification of dynamic protein−protein interfaces is one of the important tasks that needs to be undertaken during the biochemical characterization of biological processes, since receptor−ligand interactions represent one of several central events that control such vital functions as communication between cells. *Structural epitopes* governing macromolecular interactions have traditionally been determined at high-resolution by X-ray crystallography and are often defined as the molecular surface that becomes solvent-inaccessible upon complex formation. Ideally, such structural data are supplemented with mutagenesis studies to delineate the residues of the structural epitope that make the major contributions to the thermodynamic stability of the complex, that is, constitute the *functional epitope* or "hot spot" of the interaction (*1*). However, the successful identification of structural epitopes by X-ray crystallography is often hampered by the reluctance of many proteins to yield well-diffracting crystals, as exemplified by the relatively few structures determined for glycoproteins and flexible modular proteins. In these cases, the protein−protein interfaces can often be partly identified at medium resolution using a chemical protection assay by which the residues residing at the structural epitope gain resistance toward chemical modification upon complex formation (*2*, *3*). The general applicability of this method in mapping protein−protein interactions is, however, restricted by the specificity of the chemicals typically employed (e.g., acetic anhydride, tetranitromethane, cyclohexanedione, or diethylpyrocarbonate) that can target only a minor fraction of the accessible molecular surface. Such protein modifications may also perturb the conformation of the complexes under study, thus enforcing their dissociation. An attractive approach that avoids many of these shortcomings is to monitor changes in the rates of amide hydrogen exchange upon complex formation, a kinetic parameter correlated to the changes in solvent accessibility of the molecular surface. Such changes in exchange rates can be measured by mass spectrometry (*4*). A unique advantage of this method is the ability to directly distinguish between correlated and uncorrelated exchange (*5*). The former event occurs when an ensemble of otherwise protected amide hydrogens synchronously become solvent-exposed due to ligand dissociation. For the

† This work was supported by The Lundbeck Foundation, the Danish Cancer Society, the Danish Cancer Research Foundation, Carlsberg Foundation, EU Contract LSHC-CT2003-503297, Copenhagen Hospital Corporation (H:S), and Danish Biotechnology Instrument Center (DABIC).

* To whom correspondence should be addressed. Tel: +45 6550 2414. Fax: +45 6550 2467. E-mail: tjdj@bmb.sdu.dk.

‡ University of Southern Denmark.

§ Rigshospitalet.

10.1021/bi048706j CCC: $27.50
Published on Web 11/05/2004

study of protein−peptide interactions this ability is particular useful since it allows direct monitoring of complex dissociation, for which NMR is not suitable.

In the present study, we have used electrospray ionization mass spectrometry and amide $^1H/^2H$ exchange to measure simultaneously both the structural and kinetic properties of the interaction between the urokinase-type plasminogen receptor (uPAR)[1] and various linear peptide ligands that are potent antagonists of the uPA−uPAR interaction (*6*). It is, however, imperative for the further refinement of these compounds to evaluate their eligibility for transition into smaller peptidomimetics by rational drug design. The glycolipid-anchored uPAR (*7*) is involved in the generation of pericellular plasmin by confinement of the urokinase-type plasminogen activator (uPA) to the cell surface (*8*, *9*). This process is accomplished by the specific, high-affinity interaction ($K_d \approx 0.5$ nM) between uPAR and the growth factor-like module of uPA. Initial insight into the molecular basis for this receptor−ligand interaction has been obtained through studies of protection against chemical modification, through photoaffinity labeling, and by site-directed mutagenesis (*3*, *10*−*13*). Since extracellular plasminogen activation has an established role in the tissue remodeling processes that accompany cancer invasion (*14*), therapeutic intervention strategies aimed at controlling cancer dissemination by targeting the uPA−uPAR interaction (*6*, *9*) may provide useful supplements to traditional chemotherapy in the management of cancer patients (*15*). The multidomain structure and the heterogeneous glycosylation profile of uPAR have, however, complicated the characterization of its interaction with these ligands by traditional approaches such as crystallography and NMR.

MATERIALS AND METHODS

Materials. D_2O (99.9 atom % D) was obtained from Cambridge Isotope Laboratories (Andover, MA), and ammonium acetate-d_7 (98 atom % D) was from Aldrich Chemicals. All other chemicals and reagents were of the highest grade commercially available. Peptides were synthesized, purified, and characterized as reported previously (*6*, *10*).

Protein Preparations. The growth factor-like module of human urokinase (GFD_{1-45}) was expressed by the *Drosophila* S2 cell expression system from Invitrogen (Groningen, The Netherlands) with pMT/V5−His as the expression vector. Recombinant protein was purified from the conditioned medium by ligand-affinity chromatography using immobilized human uPAR (residues 1−283) followed by reversed-phase chromatography. Approximately 50% of the purified GFD_{1-45} contained the naturally occurring fucosylation (*16*) on Thr^{18}, as revealed by the monoisotopic masses of 5019.28 and 5165.36 Da determined by ESI-MS. Human uPAR mutants were expressed in either CHO cells (residues 1−277) or *Drosophila* S2 cells (residues 1−283) and purified from the conditioned media by immunoaffinity chromatography (monoclonal anti-uPAR R2-antibody) and reversed-phase chromatography as described previously (*6*, *12*). Recombinant human pro-uPA expressed in *Escherichia coli* was kindly provided by Dr. D. Saunders (Grünenthal, Germany).

Hydrogen/Deuterium Exchange. Amide $^1H/^2H$ exchange was initiated by the addition of 1 μL of a 200 μM solution of the peptide ligand (50 mM ammonium acetate buffer, pH 8.0, 0.10 M NaCl) in the presence or absence of 400 μM uPAR to 49 μL of the corresponding deuterated buffer (i.e, 50 mM d_7-ammonium acetate, pD 8.0 (uncorrected value), 0.10 M NaCl). Solutions were maintained at 6 °C and subjected to various exchange periods. At appropriate intervals, aliquots of the $^1H/^2H$ exchange solution were quenched by their addition to an equal volume of 0.5 M phosphate buffer (pH 2.2) and immediately frozen in liquid N_2. The samples were stored in liquid N_2 until analysis.

Rapid Solvent Exchange and ESI-MS Analysis. The equipment for rapid solvent exchange consists of two Applied Biosystems HPLC syringe pumps (model 140B), a Rheodyne injection valve (model 7725i), and a Valco 10-port two position air actuated valve (model C2-1000A) equipped with a C_{18} microcolumn (bed volume ~2 μL). The Valco valve is controlled by a logic module (model LOGO!, Siemens AG) by pulsing a pair of three-way solenoid valves. One pump delivered the solvent for desalting and the other that for elution. A schematic drawing of this apparatus is shown in Figure 1. Acid-quenched samples are thawed individually and injected by an ice-cold HPLC syringe into a 100 μL stainless steel loop mounted on the injection valve. To ensure accurate time control a built-in position sensing switch starts a timer program in the logic module once the handle of the injection valve is switched to the inject position. The sample is applied to and solvent-exchanged on the microcolumn for 45 s with 400 μL/min of H_2O containing 0.05% (v/v) trifluoroacetic acid (pH 2.2) after which the logic module automatically switches the Valco valve, and the sample is eluted directly to the electrospray ion source with a flow of 70% acetonitrile containing 0.05% (v/v) trifluoroacetic acid at 20 μL/min. To minimize back-exchange with the protiated solvents, the entire system is immersed in an ice/water slurry (0 °C). The desalting step removes deuterium incorporated into side chains and amino/carboxy termini, since these labile hydrogens (i.e. hydrogen attached to N, O, and S) exchange much faster than peptide backbone amide hydrogens at acidic pH (*17*).

Positive ion ESI mass spectra are acquired on Micromass quadrupole time-of-flight mass spectrometers equipped with electrospray ion sources. The instruments are calibrated using sodium iodide. ESI-mass spectra of the peptide ligands are recorded on a Q-TOF 1 mass spectrometer. The ion source parameters are: capillary voltage 3.1 kV, cone voltage 45 V, ion source block temperature 60 °C, nebulizer gas flow 20 L/h (25 °C), desolvation gas flow 400 L/h (200 °C). Nitrogen is used as nebulizer and desolvation gas. ESI-mass spectra of GFD were, however, recorded on a Q-TOF Ultima mass spectrometer operating in V-mode with ion source parameters identical to those of the Q-TOF 1 instrument, except for a cone voltage of 100 V.

THEORETICAL BASIS FOR KINETICS OF AMIDE $^1H/^2H$ EXCHANGE

Amide hydrogens engaged in intermolecular hydrogen bonding in protein−peptide complexes are generally pro-

[1] Abbreviations: uPA, urokinase-type plasminogen activator; uPAR, uPA receptor; S2-cells, Schneider 2 cells from *Drosophila melanogaster*; GFD, growth factor-like domain of uPA.

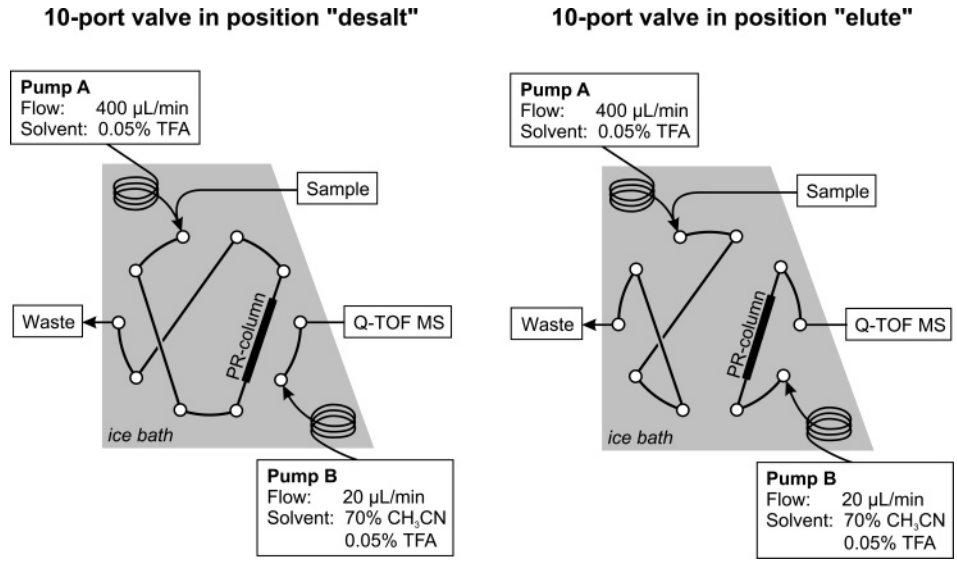

FIGURE 1: Plumbing diagram for rapid desalting apparatus.

tected against isotopic exchange with the solvent. To permit exchange, the intermolecular H-bond must be broken to allow access for the exchange catalyst ion (OD^-) (*18*). Such H-bonds may break either as a result of dissociation of the complex or during transient local structural fluctuations at the molecular interface without complete dissociation of the complex. When the backbone amide hydrogens in the peptide ligand undergo exchange because of complex dissociation, they will then exchange at their intrinsic chemical exchange rates, k_{ex}, the values of which are known from model compound studies; k_{ex} depends on sequence, pH, and temperature and can be calculated (*17*). Thus, for a model reaction,

$$RL_{HHH} \underset{k_{on}}{\overset{k_{off}}{\rightleftharpoons}} R + L_{HHH} \xrightarrow[\text{correlated}]{k_{ex}} R + L_{DDD} \qquad (1)$$

where RL_{HHH} is the complex between a protein receptor (R) and a peptide ligand (L) having three protected amides, L_{HHH} is the free ligand immediately after dissociation, L_{DDD} is the free ligand after exchange with the solvent (D_2O), k_{ex} is the intrinsic chemical amide exchange rate (s^{-1}), and k_{off} (s^{-1}) and k_{on} (M^{-1} s^{-1}) are dissociation and association rate constants for the bimolecular complex. The peptide ligand must, however, be unstructured in the uncomplexed state to undergo the fastest exchange possible, that is, limited only by the intrinsic chemical amide exchange rate.

If the average time a peptide ligand remains uncomplexed (i.e., the residence time) is significantly longer than the intrinsic half-lives of its amides, exchange will occur simultaneously at all amide groups before the peptide can enter a new complex with the receptor, that is, the hydrogen exchange is *correlated* (eq 1). In the presence of a very large excess of D_2O, this exchange reaction is considered irreversible from a practical point of view. The correlated substitution of amide protium (^1H) by deuterium (^2H) can be revealed by ESI-MS as a bimodal isotope distribution in the mass spectrum (*5*, *19*, *20*). The mass difference between the two isotope distributions represents the number of correlated exchanging amide hydrogens. Under conditions where each dissociation event of the receptor−ligand complex is intimately coupled to a correlated exchange of amide hydrogens in the ligand, the observed rate constant of exchange, k_{obs}, becomes equal to the dissociation rate constant, k_{off}, of the receptor−ligand complex:

$$k_{obs} = k_{off} \qquad (2)$$

If the exchange is completely correlated, the masses of the two isotope distributions remain constant throughout the experiment, while the abundance of the lower mass isotope distribution decreases exponentially (eq 3) and that of the higher mass isotope distribution increases correspondingly (eq 4) as exchange proceeds:

$$I_{low} = [RL]_0 \, e^{-k_{off}t} \qquad (3)$$

$$I_{high} = [L] + [RL]_0 - [RL]_0 \, e^{-k_{off}t} \qquad (4)$$

where I_{low} and I_{high} are the absolute abundances of the lower and the higher mass isotope distributions, t is the exchange time (seconds), [L] is the concentration of uncomplexed ligand, and $[RL]_0$ is the concentration of receptor−ligand complexes at $t = 0$. If the hydrogen exchange is initiated under equilibrium conditions for the receptor−ligand interaction and the concentration of the receptor is in excess of the ligand and high compared to the K_d for the interaction, the ratio of free to receptor-bound ligand is close to zero, resulting in a negligible abundance of the higher mass isotope distribution for the ligand at $t = 0$. In this case, the ratio of the abundance of the higher mass isotope distribution to the sum of the abundances follows eq 5:

$$\frac{I_{high}}{I_{low} + I_{high}} = 1 - e^{-k_{off}t} \qquad (5)$$

The dissociation rate constant, k_{off}, can be obtained by a nonlinear curve fit to this equation from the abundance ratios from mass spectra. Using abundance ratios rather than absolute abundances eliminates the error caused by fluctuations in the absolute signal intensities between experiments.

If, however, the residence time for the uncomplexed ligand is comparable to or shorter than the intrinsic half-lives of the amide hydrogens, the ligand will reassociate with its

receptor before completion of the amide hydrogen exchange. Under such conditions, numerous dissociation events may be required to complete the hydrogen exchange and the observed rate constant for the exchange of an individual amide group, k_{obs}, is calculated using the following equation:

$$k_{obs} = \frac{k_{off}k_{ex}}{k_{on}[R] + k_{ex}} \quad (6)$$

where [R] is the concentration of uncomplexed receptor protein. If a molar excess of the receptor is used, the $k_{on}[R]$ denominator term in eq 6 becomes a pseudo-first-order rate constant. Under conditions where $k_{ex} \gg k_{on}[R]$, eq 6 simplifies to eq 2. To estimate whether, upon complex dissociation, the hydrogen-bonded amides of the ligand exhibit a strictly correlated exchange, a partially correlated exchange, or uncorrelated exchange, the residence time of the peptide should be compared to the intrinsic half-lives of its amide hydrogens. Equation 7 is used to calculate the residence time, t_R:

$$t_R = \frac{[L]}{k_{off}[RL]} \quad (7)$$

The denominator represents the influx of free ligand (i.e., rate of complex dissociation), which is equal to the outflux (i.e., rate of complex formation) at equilibrium.

To allow determination of k_{off} values for receptor−ligand complexes using eq 5, it is a prerequisite that each dissociation is coupled to a correlated exchange of a sufficient number of amide hydrogens in the ligand to yield resolvable bimodal isotope distributions. It is therefore imperative to determine the kinetic limit below which the data are not easily interpreted, that is, when the probability of exchange becomes too low to generate recognizable bimodal isotope distributions. The probability of exchange, P_{ex}, for each individual amide hydrogen equals $k_{ex}/(k_{on}[R] + k_{ex})$, which is equal to k_{obs}/k_{off} (see eq 6). To illustrate this phenomenon Figure 2 shows the probability of exchange for four of the tested peptide ligands for the urokinase receptor as a function of k_{ex} for all their eight backbone amide hydrogens. At high k_{ex} values, all curves merge exhibiting a $P_{ex} \approx 1$, thus reflecting a strictly correlated exchange. At lower k_{ex} values, where $P_{ex} < 1$, there is finite possibility for reassociation of the complex before a complete exchange has occurred (i.e., partially correlated exchange). Further lowering k_{ex} values renders the exchange uncorrelated. Unfortunately, these curves cannot directly predict the transition from discrete bimodal isotope distributions to a merged single isotope distribution, since the curves pertain to individual amide hydrogens only. The algorithms developed by Arrington and Robertson are, however, well-suited to perform this task (*5*, *21*) as illustrated by the simulated mass spectra for the correlated exchange of six amide hydrogens in a peptide ligand complexed to a receptor (Figure 3). Although mass distributions tend to overlap, the probability of zero amide hydrogen exchange during a single dissociation event is very close to zero as long as $P_{ex} \geq 0.6$, and we have consequently established this value as the kinetic limit for the use of correlated exchange to determine dissociation rate constants for these protein−peptide complexes. In this respect, it is noteworthy that all the peptide ligands shown in Figure 2 have $P_{ex} \geq 0.6$ for the majority of their amide hydrogens. However, it should be emphasized that the kinetic limit will increase when the number of protected amide hydrogens decreases. In cases where the kinetic constants are unknown, the kinetic limit can be inferred by inspection of the recorded mass spectra. If a bimodal isotope distribution is observed, then any error in the determination of k_{off} (as a result of the kinetic limit) will be relatively small.

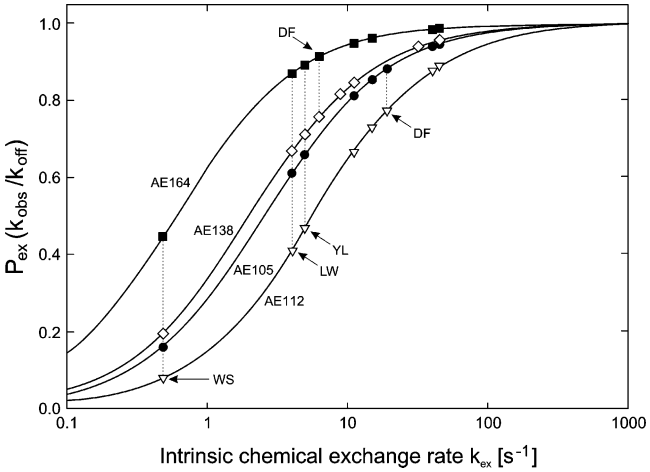

FIGURE 2: Probability of exchange. The graph shows the probability of amide hydrogen exchange ($P_{ex} = k_{obs}/k_{off}$) as a function of the intrinsic chemical exchange rate, k_{ex}, for four related peptide antagonists of the uPA−uPAR interaction (*6*). $P_{ex} = k_{obs}/k_{off} = k_{ex}/(k_{on}[R] + k_{ex})$. The rate constants for dissociation and association between uPAR and these peptide ligands have been assessed by surface plasmon resonance studies (*6*), and the intrinsic chemical exchange rates for each individual peptide backbone amide hydrogen have been calculated using the HXpep software kindly provided by Z. Zhang. The concentration of free ligand [L] present at equilibrium is calculated by $[L] = L_0 - (R_0 + L_0 + K_d \pm \sqrt{(R_0+L_0+K_d)^2 - 4R_0L_0})/2$. L_0 and R_0 are the total concentrations of receptor protein and peptide ligand. The residence time (t_R) can subsequently be derived by eq 7. As an example, the peptide antagonist AE105, having a K_d of 0.36×10^{-9} M, exhibits a $t_R = 0.39$ s if experiments are conducted at $R_0 = 8.0$ μM and $L_0 = 4.0$ μM, which yield a [L] ≈ 0.36 nM and [RL] ≈ 4.0 μM. The intrinsic chemical exchange rates (k_{ex}) at pD_{read} 8.0 for the various amide hydrogens on AE105 range from 0.5 to 45 s^{-1} corresponding to half-lives ($t_{1/2}$) between 1.4 s and 15 ms. Five amide hydrogens in AE105 have half-lives significantly shorter (by a factor of 6−25) than the residence time and undergo consequently a correlated exchange. In contrast, the C-terminal amide possessing a half-life of 1.4 s exhibits an uncorrelated exchange, since numerous dissociation events are required to complete the exchange. Finally, two amide hydrogens have half-lives that are smaller than the residence time by only a factor of ~2.5. Those amides will undergo partially correlated exchange. Since the intrinsic chemical exchange rate constant for β-cyclohexyl-L-alanine is not known, we have used that for phenylalanine instead (shown as DF in the figure for AE105 and AE138).

Data Analysis. Quantitation of the lower and higher mass populations in the ESI mass spectra was performed by nonlinear least-squares fitting of a linear combination of two Gaussian distributions (area version) (eq 8) with a fixed width (w) and a variable mean (μ) and area coefficient (A) to the isotopic peaks in the mass spectra.

$$y = \sum_{i=1}^{2} \frac{A_i}{w_i\sqrt{\pi/2}} e^{-2((x-\mu_i)/w_i)^2} \quad (8)$$

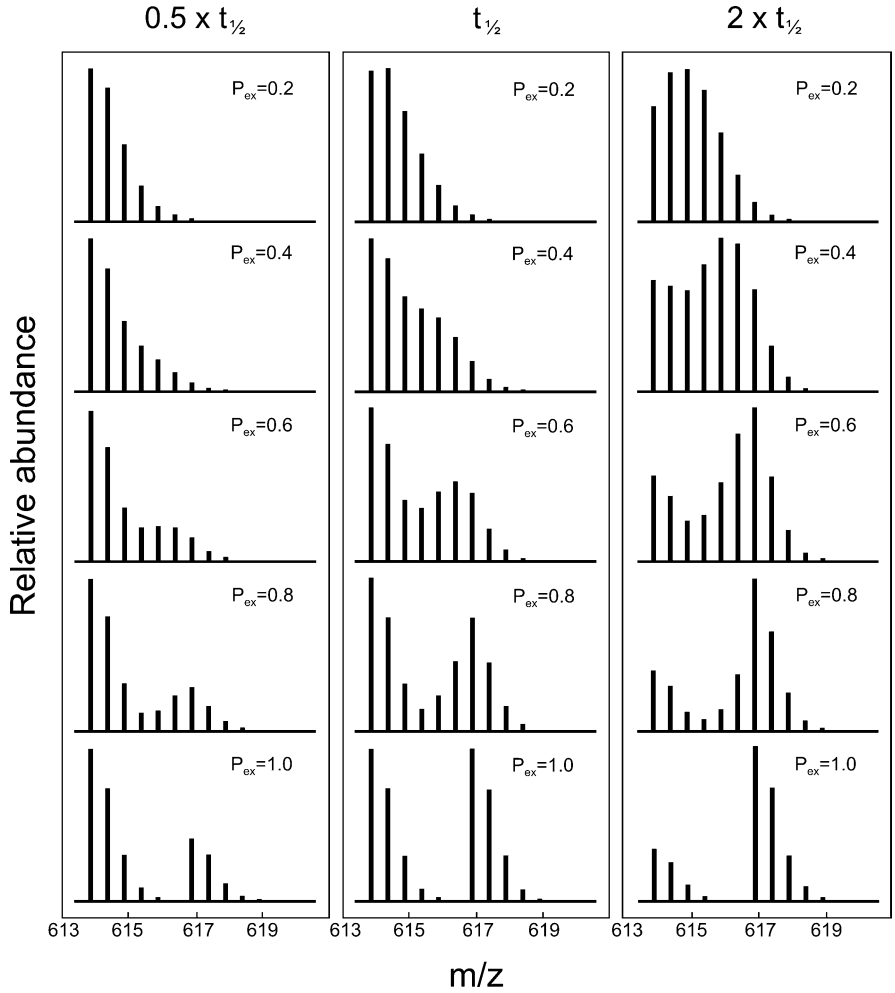

FIGURE 3: Simulated mass spectra for $^1H/^2H$ exchange. Shown are simulations of the correlated exchange for six amide hydrogens in a peptide−receptor complex having a dissociation rate constant (k_{off}) of 2.3×10^{-4} s^{-1}. This resembles the situation for the interaction between uPAR and AE105. The probability of exchange (P_{ex}) was varied from 0.2 to 1.0, and spectra corresponding to exchange times of 0.5, 1, and $2 \times t_{1/2}$ are shown. The employed simulation does not account for the deuterium incorporation that occurs while the peptide is receptor-bound, since the model cannot assign individual uncorrelated exchange rates to a subset of otherwise protected amide hydrogens that becomes transiently solvent-exposed. Consequently, the low-mass populations in the simulated mass spectra do not display any time-dependent mass increase. The simulations were carried out with the MSsimHX algorithms kindly provided by A. Robertson (*21*).

The independent variable y was the observed relative abundance (area) of the isotopic peaks. The width was determined by fitting a single Gaussian distribution with variable w, μ, and A to the isotopic distribution of the peptide ligand obtained after 20 s deuteration in the absence of uPAR. Deuterium levels (i.e., the average deuterium content) for the lower and higher mass populations of the peptide ligands were determined by the difference between their means (μ) and the average mass (i.e., centroid) of the isotopic natural abundance distribution of the corresponding peptide.

To obtain dissociation rate constants, the abundances (areas) of the lower and higher mass populations in the ESI mass spectra were determined by Gaussian fitting as described above. Subsequently, abundance ratios were plotted as a function of exchange time, and the dissociation rate constants, k_1 and k_2, and the amplitude parameter, N, were obtained from fitting biexponential kinetics (eq 9) to the data using a nonlinear least squares algorithm.

$$\frac{I_{high}}{I_{tot}} = N(1 - e^{-k_i t}) + (N - 1)(1 - e^{-k_2 t}) \qquad (9)$$

Rate constants for amide hydrogen exchange of receptor-bound peptide ligands were determined by fitting a tri-exponential equation (eq 10) to plots of deuterium levels of the lower mass population vs time.

$$\langle D \rangle = N_{fast}\, e^{-k_{fast} t} + N_{intermediate}\, e^{-k_{intermediate} t} + N_{slow}\, e^{-k_{slow} t} \qquad (10)$$

where $\langle D \rangle$ is the deuterium level. N_{fast}, $N_{intermediate}$, and N_{slow} denote the number of amide hydrogens in the each of the three kinetic categories: fast, intermediate, and slow. The rate constants for these kinetic categories are k_{fast}, $k_{intermediate}$, and k_{slow}. Because all receptor-bound peptides retain a substantial amount of protium even after prolonged periods of deuteration, it is not possible to estimate an accurate rate constant for the slowest exchanging amide hydrogens, but only to estimate upper limits. These limits are substantially lower for AE105 and AE133 compared to those for the other peptides tested, which is the direct consequence of the substantial differences in applied exchange intervals (3−4 h versus 15−30 min). For example, it is not possible to determine deuterium levels of receptor-bound AE112 at an

Table 1: Protected Amide Hydrogens and Dissociation Rate Constants in Peptide Antagonists

Ligand	Sequence[a]	Deuterium level[b]			k_{off} [10^{-4} s^{-1}][c]		t_R [s][d]
		+ uPAR	- uPAR	Δ	HDX	SPR	
AE105	D-Cha-FsrYLWS	1.1	6.9	5.8	1.2	2.3	0.4
AE112	D- F -FsrYLWS	1.5	6.8	5.3	14.6	26.0	0.2
AE164	KGSGG-D- F -FsrYLWS	5.9	11.2	5.3	37.5	36.0	1.7
AE138	KGSGG-D-Cha-FsaYLWS	4.6	11.1	6.5	6.3	12.0	0.5
AE133	KGSGG-D-Cha-FsrYLWS	4.6	11.0	6.4	0.9	2.5	0.5
GFD	1-45	23.9	34.5	10.6	nd	3.1	0.3
GFD-fuc[e]	1-45[e]	21.8	34.8	13.0	nd	3.1	0.3

[a] Amino acids are shown in the single letter code where capitals denote L-chirality and lower case D-chirality. Peptides have unmodified N- and C-termini. Cha is β-cyclohexyl-L-alanine. [b] Average deuterium content after 20 s deuteration in the presence (+) or absence (−) of uPAR and their difference are shown (Δ). For GFD, the deuteration period was 30 s. [c] Dissociation rate constants were measured by either amide hydrogen exchange (HDX) or surface plasmon resonance (SPR) for $uPAR^{wt}$ and derivatives of AE105 (*6*). The values shown for HDX correspond to $k_{1,off}$ derived by the biexponential fitting procedure using eq 10 in the Theoretical Basis for Kinetics of Amide $^1H/^2H$ Exchange section. [d] Residence time (lifetime) for uncomplexed peptide ligands as determined by eq 7 in the Theoretical Basis for Kinetics of Amide $^1H/^2H$ Exchange section using k_{off} kinetic data derived from SPR experiments. [e] Fucosylated at Thr^{18}.

exchange period much longer than 15 min, since the lower mass population then becomes too depleted to be quantified. The shortest exchange interval that can be measured from a practical point of view is 20 s of deuteration. At this time, all receptor-bound peptides have incorporated at least one deuteron, for which we can estimate the lower limits that apply for the rate constants of these fast exchanging amide hydrogens. In summary, upper and lower limits for rate constants can be estimated for the slow and fast categories, whereas rate constants in the intermediate kinetic category ($(2-42) \times 10^{-3}$ s^{-1}) can be measured directly.

Nonlinear least-squares fitting was carried out with the solver algorithm implemented in Microsoft Excel spreadsheet software (*22*). For the fitting of the Gaussian distributions, the ion abundance cutoff level was set at 2% on the relative abundance scale.

To obtain the exact number of protected amide hydrogens on the peptide ligands, it is necessary to know their isotope distributions prior to quenching and desalting. However, such knowledge is difficult to obtain because of the fast exchange of the N-terminal amide hydrogen under quenched conditions (at acidic pH, the positive charge on the N-terminus increases the exchange rate at the adjacent amide hydrogen by a factor of ~10). This means that deuterons incorporated at N-terminal amide groups are readily lost during desalting, and it is thus not possible to determine whether this amide group was deuterated or protiated before quenching. For this reason, we have not adjusted the observed deuterium levels for any deuterium loss. It should, however, be emphasized that corrections for deuterium loss generally are needed for experiments comparing different peptic fragments.

Peptides with deuterium contents less than 50% will incorporate deuterons when they are exposed to the 1:1 (v/v) mixture of deuterium and quenching buffer and those with more than 50% will loose deuterons. In addition, a certain amount of deuterium loss occurs during the subsequent desalting steps. In the present experiments, the number of protected amide hydrogens is determined by the average mass difference between two molecular populations, one with a deuterium content lower than 50% and the other with a deuterium content ~85%. The latter population will always experience the highest net deuterium loss during quenching and desalting, which inevitably leads to a reduction in the average mass difference between the two populations. The observed mass differences therefore represent the minimum number of protected amide hydrogens.

RESULTS

Determination of the Minimum Number of Amide Hydrogens in a Peptide Antagonist Exhibiting Reduced Exchange Rates as a Consequence of uPAR Ligation. High-affinity nine-mer peptide antagonists of the uPA−uPAR interaction have recently been developed via a combination of phage-display technology, affinity maturation by combinatorial chemistry, and affinity measurements by surface plasmon resonance (*6*, *10*). The contributions of the individual amino acid side chains to this high-affinity interaction have been explored by a systematic alanine scanning of the peptide antagonists (*6*), and a gross topological mapping of the intermolecular interface with uPAR has been obtained by photoaffinity labeling (*10*, *11*) and site-directed mutagenesis (*6*). To further address the involvement of the peptide backbone on this interaction, we have now undertaken a thorough study by amide $^1H/^2H$ exchange combined with ESI mass spectrometry. The sequences of the uPAR peptide ligands studied here are shown in Table 1.

The minimum number of peptide amide hydrogens involved in the interaction with uPAR is revealed by the average mass difference between the isotopic distributions acquired after 20 s deuteration in the presence or absence of a 2-fold molar excess of uPAR. For AE105, a mass difference of 5.8 Da is consistently observed for such analyses (compare Figure 4, panels b and c). This indicates that at least six amide hydrogens out of a total of eight are directly involved in this interaction. An equivalent analysis for AE133, which represents an extended analogue of AE105, is also shown in Figure 4 (right column). The N-terminal sequence extension of AE133 (i.e., KGSGG-) is unlikely to be directly engaged in the interaction with uPAR, since the dissociation and association rate constants determined for its interaction with uPAR by surface plasmon resonance are similar to those of AE105 (Table 1) (*6*). The ESI mass spectra recorded for AE133 after amide $^1H/^2H$ exchange for 20 s in the presence of uPAR further substantiate this notion, since the average mass of AE133 was shifted by 4.6 Da relative to the average mass of the isotopic natural abundance

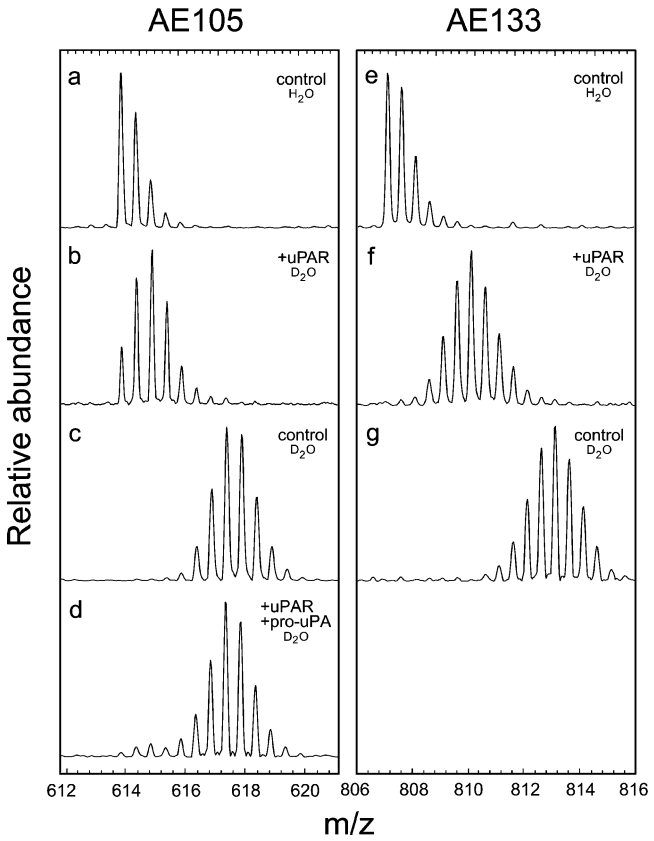

FIGURE 4: Amide $^1H/^2H$ exchange on two high-affinity peptide antagonists as a function of receptor occupancy. Shown are ESI mass spectra for the doubly protonated AE105 (D-Cha-FsrYLWS, left column) and AE133 (KGSGGD-Cha-FsrYLWS, right column) before deuteration (a, e) and after 20 s of deuteration in the presence (b, f) or absence (c, g) of uPAR or pro-uPA·uPAR complexes (d). During the exchange conditions, 4 μM peptide was incubated with 8 μM uPAR or pro-uPA·uPAR complexes.

distribution (compare Figure 4, panels e and f). The corresponding shift for AE105 is only 1.1 Da (compare Figure 4, panels a and b). This reflects that none of the "added" amide hydrogens in the N-terminal extension of AE133 is protected against exchange due to specific engagements in hydrogen bonding to uPAR. In comparison, the C-terminal region of AE133, which is identical to AE105, contains seven protected amide hydrogens as evident from the mass difference of 6.4 Da between the isotopic distributions of AE133 in the presence or absence of uPAR (compare Figure 4, panels f and g). Other peptide derivatives of AE105 tested in this study exhibit a similar number of protected amide hydrogens when they form complexes with uPAR (Table 1).

The specificity of the interaction between AE105 and uPAR was confirmed by preincubating uPAR with a 2-fold molar excess of its natural ligand pro-uPA prior to addition of AE105. The recorded isotope distributions of AE105 in the presence or absence of a 2-fold molar excess of uPAR·pro-uPA complex are essentially identical (compare Figure 4, panels c and d) showing that complexed uPAR does not offer any protection against the amide $^1H/^2H$ exchange of AE105. This corroborates previous data on the antagonistic properties of AE105 (*6*) and ensures that our exchange experiments are indeed probing structurally well-defined interactions between uPAR and these peptide ligands.

Determination of Dissociation Rate Constants for uPAR−Peptide Antagonist Complexes. Mass spectra obtained for

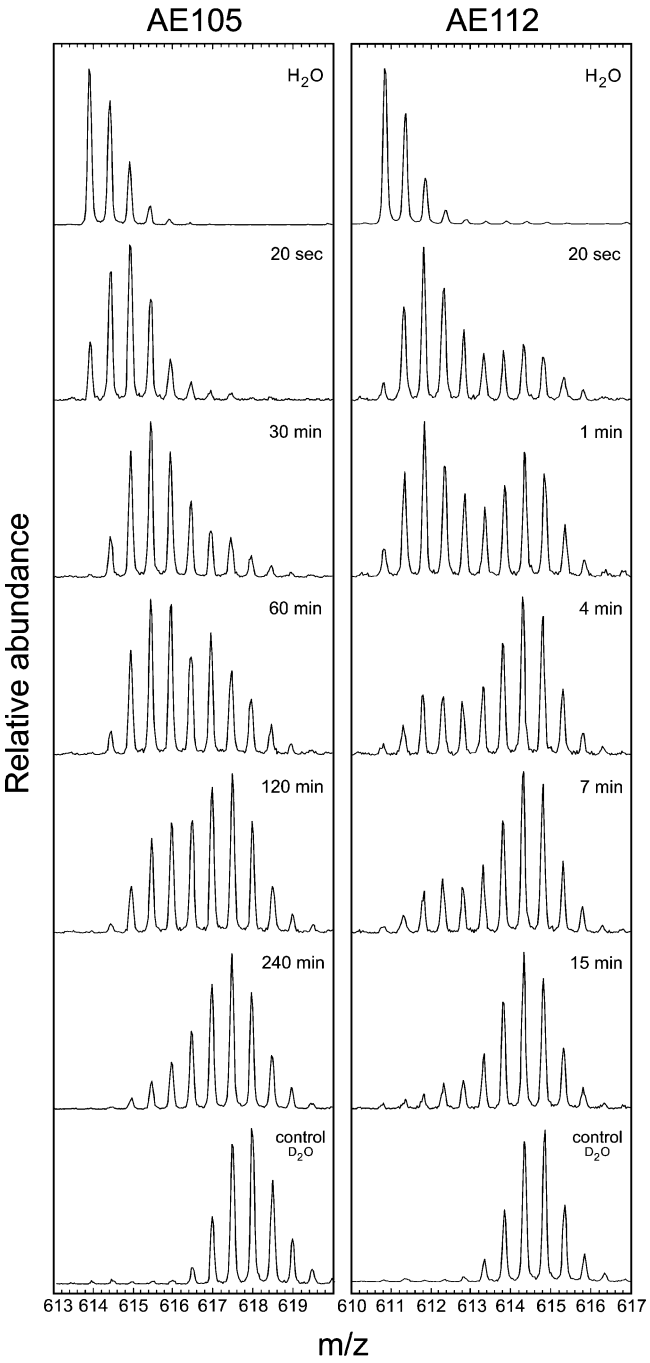

FIGURE 5: Time course for amide $^1H/^2H$ exchange on two different peptide complexes with uPAR having widely different stabilities. The ESI mass spectra for the doubly protonated peptide ligands obtained after various deuteration periods in the presence of uPAR are shown for AE105 (D-Cha-FsrYLWS, left column) and AE112 (D-F-FsrYLWS; right column). Spectra labeled H_2O were obtained before deuteration in the absence of uPAR and spectra labeled control were obtained after 20 s deuteration in the absence of uPAR. During the exchange conditions, 4 μM peptide was incubated with 8 μM uPAR.

time-course incubations in D_2O of the peptide ligands AE105 and AE112 in the presence of uPAR are presented in Figure 5. For AE105, a single isotopic envelope dominates the spectrum at short incubation times (20 s), but upon prolonged incubation, an isotope distribution at higher mass appears. This leads to a bimodal isotope distribution with both modes nearly equally populated after approximately 60 min. By contrast, an equivalent bimodal distribution is present after

only 1 min incubation of AE112. This peptide is derived from AE105 by a single substitution (cyclohexylalanine replaced by phenylalanine), which severely compromises its affinity for uPAR as measured by surface plasmon resonance (Table 1) (*6*). Since the higher mass populations in Figure 5 (representing correlated exchange) are formed with rate constants equivalent to those of complex dissociation (see the Theoretical Basis for Kinetics of Amide $^1H/^2H$ Exchange section), it is beyond any doubt that AE112·uPAR complexes therefore must have a considerably higher off-rate than the AE105·uPAR complexes in these experiments.

To determine the actual dissociation rate constants (k_{off}), the mass data for AE105 and AE112 were first fitted to monoexponential dissociation kinetics according to eq 5 in the Theoretical Basis for Kinetics of Amide $^1H/^2H$ Exchange section, which yielded a value of 1.3×10^{-4} s^{-1} for AE105 and 5.5×10^{-3} s^{-1} for AE112. However, subsequent evaluation of this interaction model revealed a rather imperfect fit to the data measured for AE112 in particular (Figure 6A). Refitting the data with biexponential dissociation kinetics according to eq 9 in the Theoretical Basis for Kinetics of Amide $^1H/^2H$ Exchange section improved the fit for AE105 only marginally. The derived biphasic kinetic constants are $k_{1,off} = 1.2 \times 10^{-4}$ s^{-1} (~95% of total amplitude) and $k_{2,off} = 5.2 \times 10^{-2}$ s^{-1} (~5% of total amplitude) showing that the stability of AE105·uPAR^{wt} complex is primarily dominated by the slow dissociating component. By contrast, analysis of AE112·uPAR complexes using the biphasic model dramatically improves the quality of the fitting (Figure 6A) generating nearly equal amplitudes for a fast and a slow dissociating component. The derived kinetic constants for AE112 are $k_{1,off} = 1.5 \times 10^{-3}$ s^{-1} (~45% of total amplitude) and $k_{2,off} = 3.0 \times 10^{-2}$ s^{-1} (~55% of total amplitude). The optimal fits to biphasic kinetics for AE112 indicate the occurrence of two dissociation/unfolding events between this peptide and uPAR^{wt} in solution, but the molecular basis for this remains to be solved. Interestingly, we find a positive correlation between the dissociation rate constant of the slow component and the amplitude of the fast component for several pairs of receptor−ligand complexes using this fitting procedure (Figure 6B). Consistent with the fact that the estimated k_2 dissociation rate constants are too fast to be assessed experimentally by surface plasmon resonance, we find a reasonable good agreement between the k_1 dissociation rate constants determined by amide $^1H/^2H$ exchange in solution and those derived by surface plasmon resonance using immobilized uPAR (Table 1).

Comparison of Exchange Kinetics for AE105 in Complex with Different uPAR Mutants. The isotopic distributions for AE105 obtained after various periods of deuteration in the presence of different uPAR mutants are shown in Figure 7. The attainment of a bimodal isotope distribution for AE105, where both modes are approximately equally populated, is observed after widely different incubation times for the various uPAR mutants: 60 min for uPAR^{wt} and 15 min for uPAR^{D254A} compared to only 0.25 min for uPAR^{H249A}. Since the rate of formation of the higher mass populations is equal to the rate of complex dissociation, it is evident that the two mutants H249A and D254A have higher dissociation rate constants than wild-type uPAR. The double mutant H249A/H251A yields only a single isotopic envelope, which is identical to the one obtained in the absence of uPAR,

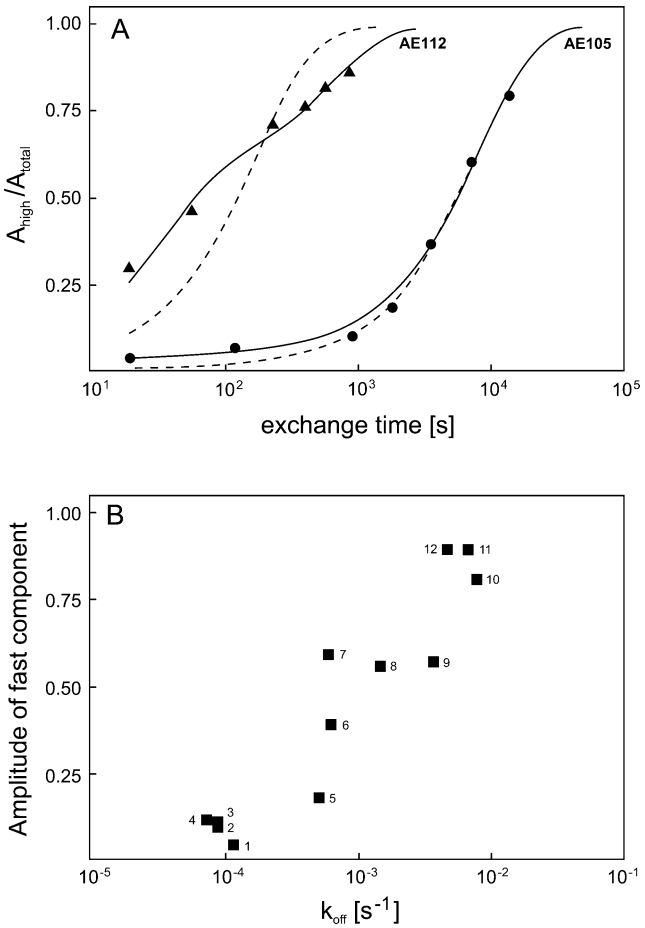

FIGURE 6: Evaluation of the kinetic fits to the dissociation of AE105 and AE112. In panel A is shown the ratio of the abundance of the higher mass population to the sum of the higher and lower mass populations as a function of exchange time for AE105 (●) and AE112 (▲). Experimental data as well as fits to monophasic (dotted lines) and biphasic (solid lines) kinetics are shown. Panel B illustrates the correlation between the amplitude of the fast dissociating component and the dissociation rate constant of the slow component for 11 different pairs of receptor−ligand complexes. The identities of these complexes are as follows: (1) AE105·uPAR^{wt}; (2) AE133·uPAR^{wt}; (3) AE105·uPAR^{K62A}; (4) AE105·uPAR^{N259A}; (5) AE105·uPAR^{D254A}; (6) AE138·uPAR^{wt}; (7) AE105·uPAR^{L55A}; (8) AE112·uPAR^{wt}; (9) AE164·uPAR^{wt}; (10) AE105·uPAR^{F256A}; (11) AE105·uPAR^{H249A}; (12) AE105·uPAR^{H249K}.

demonstrating that this mutant offers no measurable protection on AE105. These findings corroborate the binding kinetics determined by surface plasmon resonance (*6*). Dissociation rate constants (k_{off}) for the various uPAR mutants measured by amide $^1H/^2H$ exchange as well as by surface plasmon resonance are shown for comparison in Table 2. It is comforting to find that the k_{off} values obtained by surface plasmon resonance and amide $^1H/^2H$ exchange differ only by approximately 2−3-fold, despite the obvious distinctions in the two methodologies, and both methods rank the mutants into the same kinetic categories (see Table 2).

The numbers of amide hydrogens in AE105 that gain protection against exchange upon binding to uPAR mutants are listed in Table 2. Interestingly, these receptor mutants offer almost similar levels of protection on AE105 (5.7−5.9) irrespective of their widely differing dissociation rate constants. The one exception is F256A, which presents a moderately reduced level of protection on AE105 (5.4). This particular mutant also possesses the highest dissociation rate

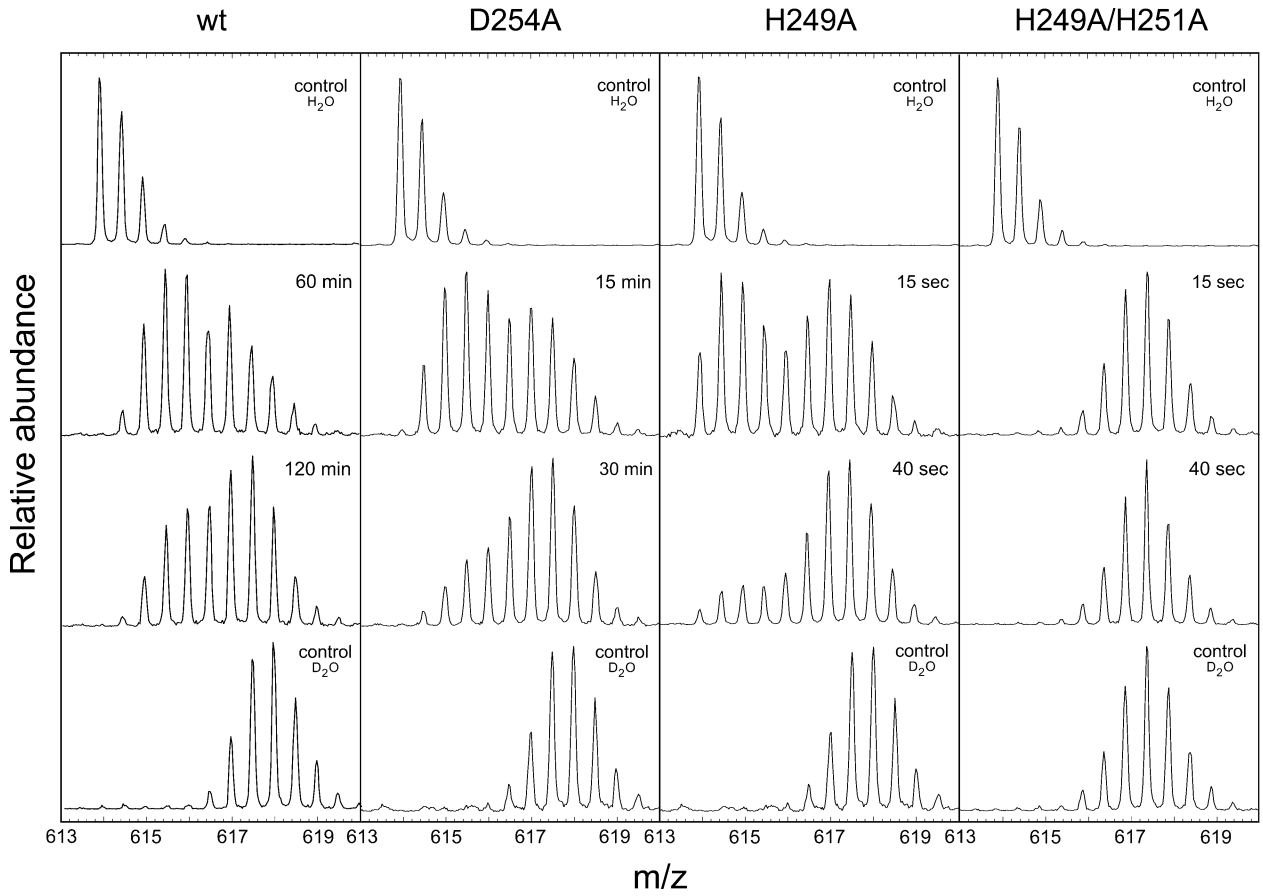

FIGURE 7: Time course for amide $^1H/^2H$ exchange of complexes between AE105 and different uPAR mutants. The ESI mass spectra for the doubly protonated AE105 were obtained after various periods of deuteration in the presence of a 2-fold molar excess of either $uPAR^{wt}$ or selected mutants. Spectra labeled H_2O were obtained before deuteration in the absence of uPAR, whereas spectra labeled control were obtained after 20 s deuteration in the absence of uPAR. The data for $uPAR^{H249A/H251A}$ was recorded after quenching in formic acid, which increased the back-exchange during desalting thereby lowering the overall deuterium incorporation. During the exchange conditions, 4 μM peptide was incubated with 8 μM uPAR.

constant for AE105 (Table 2) and furthermore yields the highest intermediate exchange rate for receptor-bound AE105 of all mutants tested (Table 3). The acceleration of the exchange rates for bound AE105 strongly indicates that this mutation promotes local distortional motions at the molecular interface of AE105·$uPAR^{F256A}$.

Deuterium Levels for the Higher Mass Populations Show That Not All Amide Hydrogens Undergo Correlated Exchange upon Complex Dissociation. Levels of incorporated deuterium in four peptide ligands, AE105, AE112, AE164 and AE138, are presented as a function of deuteration time in Figure 8. A close inspection of the deuterium levels for the higher mass populations represented by the solid symbols in Figure 8 reveals that all peptide ligands (excluding AE164) surprisingly incorporate fewer deuterons than the corresponding uncomplexed controls (broken lines). This is illustrated by the fact that even after 60 min of deuteration the difference between the higher mass populations for AE105 in the presence and absence of uPAR is still 1.0 Da (Figure 8A) suggesting that one otherwise protected amide hydrogen is not undergoing correlated exchange in the uncomplexed state. Inspection of Figure 2 in the Theoretical Basis for Kinetics of Amide $^1H/^2H$ Exchange section reveals that the most likely candidate to undergo uncorrelated exchange is the C-terminal WS amide hydrogen, since it has by far the lowest probability of exchange ($P_{ex} = 0.16$) of all the amide hydrogens in AE105. Accordingly, its intrinsic chemical half-life of exchange ($t_{1/2} = 1.4$ s) is considerably longer than the residence time for the uncomplexed AE105 ($t_R = 0.4$ s). As a result of this, only a small fraction of dissociated AE105 molecules will succeed in exchanging their WS amide hydrogen within the residence time, and several dissociation events are consequently required to accomplish a complete exchange. Assuming that exchange of WS occurs only upon complex dissociation, thus ignoring any exchange that may occur while AE105 is receptor-bound, its theoretical half-life in the presence of uPAR should be ~5.3 h (calculated using eq 6). This value is concordant with the experimental half-life of the WS amide hydrogen (~4 h) determined in the presence of uPAR suggesting that very limited exchange of WS actually occurs while AE105 is receptor-bound.

The deuterium level for the higher mass population of AE112 is closer to the maximum level than AE105 (Figure 8A). Thus, the WS amide hydrogen of AE112 exchanges faster than that of AE105. Their theoretical half-lives of 56 min and 5.3 h, respectively, are consistent with this observation.

Interestingly, AE164 is the only peptide for which the deuterium level of the higher mass population resembles that of the control (Figure 8B). The completion of the WS amide hydrogen exchange in AE164 signifies that the uPAR·AE164 complex is more labile than the corresponding uPAR·AE112 complex. Accordingly, the dissociation rate constant of the

Table 2: Protected Amide Hydrogens and Dissociation Rate Constants Determined for AE105 in Complex with uPAR^{wt} and Various Mutants

uPAR mutation	deuterium level[a]			k_{off} [10^{-4} s^{-1}][b]	
	+uPAR	−uPAR	(Δ)	HDX	SPR
wt	1.1	6.9	5.8	1.2	3.3
Neutral Mutations					
N259A	1.1	6.8	5.7	0.7	3.3
K62A	1.1	6.8	5.7	0.9	2.2
Moderately Destabilizing Mutations					
D254A	1.1	6.9	5.8	5.1	11.6
Y57A	1.2	6.9	5.7	4.6	6.1
L55A	1.2	7.0	5.8	6.0	11.1
Highly Destabilizing Mutations					
H249A	1.1	7.0	5.9	67.3	34.4
F256A	1.6	7.0	5.4	78.0	48.9
H249A/H251A[c]	6.2	6.2	0.0	>2000	>500

[a] Average deuterium content after 20 s deuteration in the presence (+) or absence (−) of uPAR and their difference are shown (Δ). For H249A, the deuteration period was only 15 s. [b] Dissociation rate constants were measured by amide hydrogen exchange (HDX) for AE105 in complex with uPAR^{wt} or the indicated uPAR mutants. The values shown for HDX correspond to $k_{1,off}$ derived by the biexponential fitting procedure using eq 10 in the Theoretical Basis for Kinetics of Amide $^1H/^2H$ Exchange section. The dissociation rate constants determined by surface plasmon resonance (SPR) were measured between the indicated uPAR mutants in solution and AE133 immobilized to the sensor chip by its amino-terminal lysine. As shown in Table 1, the k_{off}'s determined by SPR for immobilized uPAR and AE105 or AE133 in solution are comparable. [c] These data were obtained using formic acid to quench exchange before desalting. This caused a slightly higher overall back-exchange during the experiment.

Table 3: Rate Constants for Amide Hydrogen Exchange of Receptor-Bound Peptides Ligands

code	kinetic category[a]		
	fast [s^{-1}]	intermediate [s^{-1}] × 10^{-3}	slow [s^{-1}] × 10^{-5}
Antagonist·uPAR^{wt}			
AE105	1 (>0.2)	1 (8)	5 (<8)
AE112	1 (>0.2)	1 (18)	5 (<67)
AE164	6 (>0.2)	1 (2)	4 (nd)
AE138	4 (>0.2)	1 (25)	6 (<50)
AE133	4 (>0.2)	1 (7)	6 (<8)
AE105·uPAR^{mut}			
L55A	1 (>0.2)	1 (8)	5 (<50)
Y57A	1 (>0.2)	1 (8)	5 (<50)
K62A	1 (>0.2)	1 (7)	5 (<10)
H249A	1 (>0.2)	1 (18)	5 (nd)
D254A	1 (>0.2)	1 (8)	5 (<33)
F256A	1 (>0.2)	1 (42)	5 (nd)
N259A	1 (>0.2)	1 (7)	5 (<8)

[a] The number of amide hydrogens exchanging with the rate constant (s^{-1}) shown in parentheses. (nd) = not determined. Adjustment for deuterium loss or gain under quench conditions according to the procedure of Zhang and Smith (*38*) caused only insignificant changes in the deuterium levels in the data series. No adjustments have consequently been made.

uPAR·AE164 complex is 2-fold faster and the association rate constant 9-fold slower than those of uPAR·AE112 as assessed by surface plasmon resonance (*6*), which translate into a theoretical half-life of approximately 7 min for the WS amide hydrogen.

The lifetime of the uncomplexed state (i.e., the residence time) constitutes a short well-defined exposure of the peptide to deuterated solvent and can as such be used to probe the

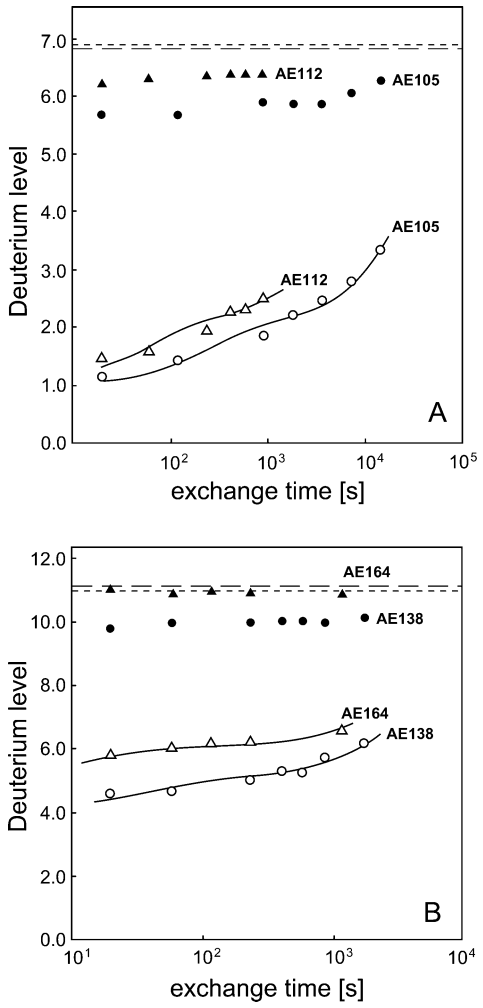

FIGURE 8: Deuterium incorporation as a function of deuteration time. Panel A show the deuterium levels obtained for the nine-mer antagonists AE105 (●,○) and AE112 (▲, △), whereas deuterium levels for the 14-mer extended versions AE138 (●,○) and AE164 (▲, △) are shown in panel B. Filled symbols represent deuterium levels for peptides that have been dissociated from uPAR and subsequently have undergone correlated exchange (corresponds to the higher mass populations). The open symbols represent the deuterium levels for receptor-bound peptide ligands that have not yet been dissociated from the receptor (corresponds to the lower mass populations). The solid lines show the fit with the kinetic equation (eq 10) to the data, and the broken lines depict the deuterium level measured in the absence of receptor. In panels A and B, the upper broken lines represent AE105 and AE164, and the lower broken lines represent AE112 and AE138, respectively.

structure of the transiently free peptides. If a peptide ligand adopts a stable, hydrogen-bonded conformation, for example, β-hairpin or α-helix, after receptor dissociation the amide hydrogens that are engaged in intramolecular hydrogen bonding will not exchange in a correlated manner. The fact that the majority of amide hydrogens on the peptide ligands tested in this study undergo correlated exchange indicates that the uncomplexed peptides are either unstructured or adopt a labile conformation that unfolds rapidly compared to the dissociation rate constant of the peptide−uPAR complex. The incomplete correlated exchange observed for some of the peptide ligands is thus best explained by the very slow intrinsic chemical exchange rate of the C-terminal WS-amide hydrogen. Despite the relatively long intrinsic chemical half-life of this particular amide hydrogen ($t_{1/2}$ =

1.4 s), it will nevertheless exchange more than 99% in the control experiment (i.e., after 20 s D_2O incubation in the absence of uPAR).

Deuterium Levels for the Lower Mass Populations Report on Exchange Mechanisms That Occur While the Peptide Ligands Are Receptor-Bound. As evident from Figure 8, the lower mass isotope distributions of all peptides tested demonstrate a time-dependent increase of the deuterium level reflecting a uncorrelated $^1H/^2H$ exchange. This phenomenon can also be recognized by the gradual mass shifts of the left isotope distributions toward higher masses (e.g., AE105 in Figure 5), which is caused by an uncorrelated exchange mechanism that is operational while the peptide ligands remain bound to uPAR. The amide hydrogens in the receptor-bound peptide ligands have their own individual exchange rate constants. Although these constants cannot be determined separately, their range and distribution can be assessed by fitting parameters in eq 10 to the experimental data (Table 3).

For receptor-bound AE105 and AE112, a fast exchange of one amide hydrogen is observed ($k_{obs} > 0.2\ s^{-1}$), while a second amide hydrogen exchanges substantially more slowly ($k_{obs} = 8.3 \times 10^{-3}$ and $k_{obs} = 1.8 \times 10^{-2}\ s^{-1}$, respectively). The remaining five amide hydrogens exhibit an extremely slow exchange with average $k_{obs} < 8 \times 10^{-5}$ and $7 \times 10^{-4}\ s^{-1}$ for AE105 and AE112, respectively (Table 3). As noted earlier, the difference in upper limits between the rate constants of AE105 and AE112 is mainly caused by their widely differing exchange times.

As expected, the N-terminal extension (KGSGG-) of derivatives of AE105 (i.e., AE133, AE164, and AE138) adds fast exchanging amide hydrogens to the receptor-bound peptides. Six amide hydrogens in AE164 and four in AE138 and AE133 thus belong to the fast exchanging category with rate constants greater than $0.2\ s^{-1}$. Both short and extended versions of the peptide antagonists contain a single amide hydrogen having a medium exchange rate constant. Interestingly, the extended versions of the tight binding antagonists (i.e., AE133 and AE138) have one additional amide hydrogen in the slow kinetic category compared to those of the shorter peptide ligands. A plausible cause for this distinction is the elimination of the positive charge of the ammonium ion of the originally N-terminal aspartic acid in the extended versions, which significantly lowers the intrinsic chemical exchange rate for the adjacent aspartic acid−β-cyclohexyl-L-alanine (Cha) amide hydrogen at acidic pH (see Figure 2). This reduces the extent of back-exchange during desalting and elution allowing us to include this position in the determination of receptor-mediated protection on the exchange kinetics.

From these data, we can now estimate the lower limit for the protection factors (PF) for the slowly exchanging amide hydrogens in AE105 and AE133 by dividing the average intrinsic chemical exchange rate constant by the upper limit of k_{obs} (i.e., PF > $18\ s^{-1}/8 \times 10^{-5}\ s^{-1}$, which yields a PF > 10^5). The slow category of amide hydrogens in AE105 and AE133 thus typically exhibits protection factors greater than 10^5 when they are engaged in complex formation with uPAR. For comparison, the PFs for the slowly exchanging amide hydrogens in native equine cytochrome *c* range from about 10^3 to 10^{10} with a median of 10^5, and more importantly, those hydrogens protected from exchange by PFs greater than 10^3 are all engaged in the formation of well-defined hydrogen bonds (*18*).

Hydrogen exchange by way of local structural fluctuation depends on dynamic structural motility of the main chain, which tends to be slow for hydrogens that are adjacent to immobile and tightly packed structures (*18*). A mutation that increases the flexibility of the polypeptide main chain locally will as a consequence also cause acceleration of amide hydrogen exchange in close proximity to the mutated residue. By analogy, we expect that mutations in peptide−receptor interfaces that decrease complex stability generally are correlated to increased main chain flexibility and therefore induce accelerated amide $^1H/^2H$ exchange at the interface of the complex.[2] Concordantly, substitution of D-arginine in AE133 by D-alanine increases the complex dissociation rate constant by about 5-fold (compare AE133 with AE138 in Table 1), and this is reflected by a 4-fold increase in the intermediate rate constant for amide $^1H/^2H$ exchange (Table 3). Since the intrinsic chemical exchange rate for the alanine residue is lower than that of the arginine residue, the observed increase in the intermediate exchange rate for AE138 clearly reflects increased local structural fluctuations induced by the mutation. As demonstrated previously, single site mutations in uPAR that impair the stability of the uPAR·AE105 complex, for example, $uPAR^{F256A}$ and $uPAR^{H249A}$, lead to a similar proportional increase in the uncorrelated exchange rate of receptor-bound AE105.

In summary, the high protection factors observed for AE133 and AE105 and their lower intermediate exchange rates reflect a relative rigid intermolecular interface between these tightly embedded peptide ligands and $uPAR^{wt}$.

Analysis of the uPAR-Binding Module in uPA. The multidomain structure of urokinase-type plasminogen activator (uPA), the cognate protein ligand for uPAR, consists of three individual modules: a growth factor domain (GFD), a kringle domain, and a serine protease domain. All structural requirements for maintenance of high affinity toward uPAR are confined within the small GFD module of uPA, where residues residing in the flexible Ω-loop of the GFD in particular (i.e., residues 20−30) are implicated in its interaction with uPAR (*9*, *23*). Human uPA contains an O-linked fucose attached to Thr^{18} in the GFD module (*16*), and this modification is apparently indispensable (*24*) for an alleged growth promoting effect of uPA on the osteosarcoma cell line SaOS-2 (*25*). The three-dimensional solution structure of GFD, along with the kringle domain, has been determined by NMR spectroscopy (*26*), but a structure for the corresponding uPAR·GFD complex remains yet to be solved. To investigate the interaction between uPAR and GFD further, we have now probed the structure of complexed and uncomplexed GFD by amide $^1H/^2H$ exchange.

A purified preparation of recombinant GFD modules (residues 1−45), containing a partial processing of Thr^{18} with

[2] The early mechanistic events in uPAR−peptide complex dissociation are assumed to constitute a number of consecutive disruptions of hydrogen bonds associated with solvation of the separated hydrogen bond donor/acceptor pairs. As mentioned previously, dynamical structural motions at the molecular interface are intimately linked to transient hydrogen bond cleavages, which eventually leads to complex dissociation. Uncorrelated amide $^1H/^2H$ exchange therefore reports directly on the transient distortional motions causing hydrogen bond breakage.

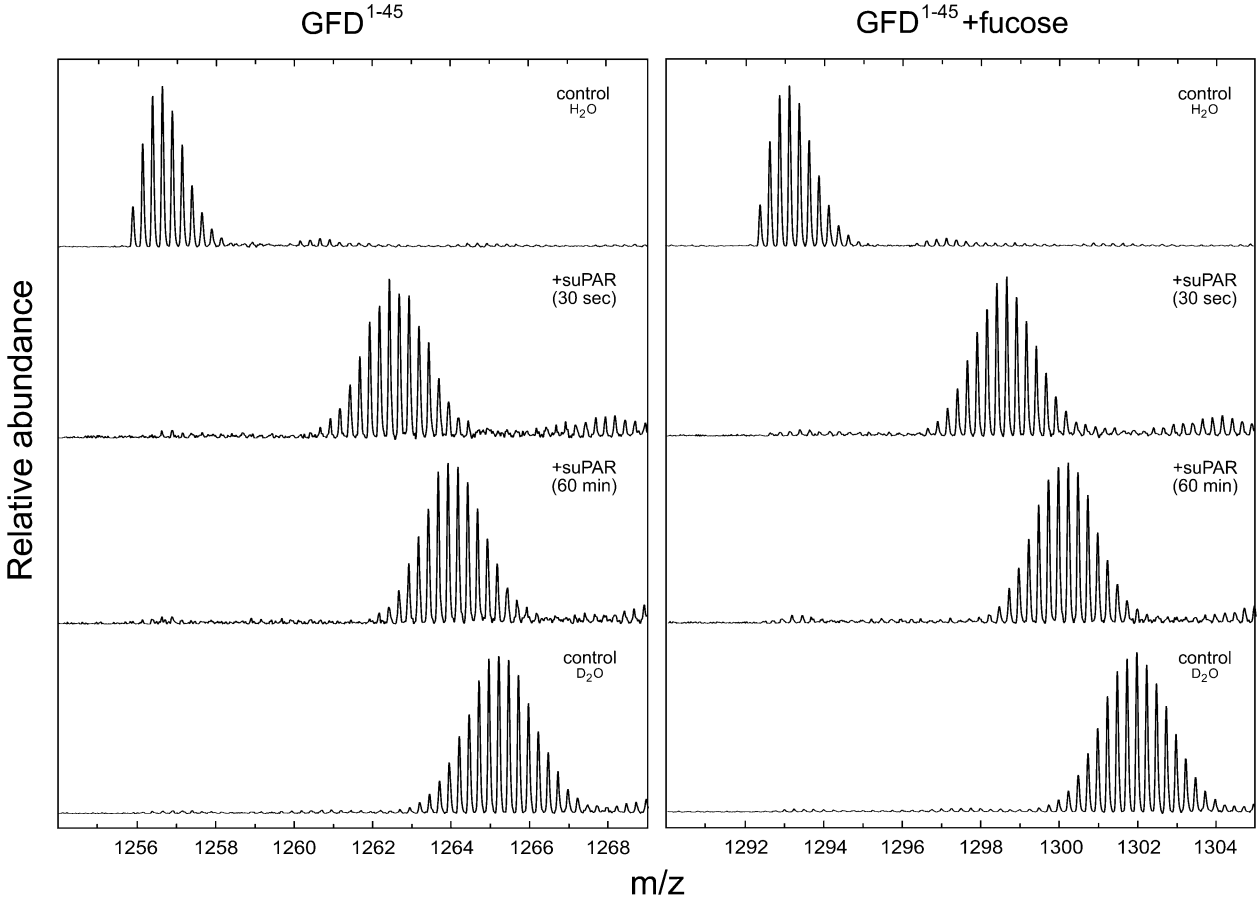

FIGURE 9: uPAR-mediated protection of amide hydrogens in GFD^{1-45} with and without fucosylation at Thr^{18}. ESI mass spectra for the quadruply protonated GFD^{1-45} without (left panel) and with (right panel) fucose attached to Thr^{18} are shown as a function of deuteration time in the presence of $uPAR^{wt}$. Spectra labeled H_2O were obtained before deuteration in the absence of uPAR, whereas spectra labeled control were obtained after 30 s of deuteration in the absence of uPAR.

the naturally occurring O-linked fucose (*16*), was therefore incubated in deuterated buffer with or without the presence of a 2-fold molar excess of uPAR. This particular experimental setup allows possible impacts of the fucosylation on the exchange kinetics of the GFD to be assessed directly by comparison of the mass shifts observed for the two forms in a single ESI mass spectrum (Figure 9). In the absence of uPAR approximately 35 deuterons are rapidly (i.e., within 30 s) incorporated into both forms of GFD (Table 1). Because prolonged incubations did not result in a further increase of their deuterium content (data not shown), these experiments indicate that the isolated GFD modules adopt a highly flexible structure in solution with a very limited self-contained protection against solvent exchange.[3] In the presence of a molar excess of uPAR, this incorporation is reduced to 24 deuterons in GFD and only 22 in the fucosylated GFD. Complex formation with uPAR thus confers an average protection corresponding to 11 amide hydrogens in the nonfucosylated GFD compared to 13 in the fucosylated GFD. Intriguingly, the covalently attached fucose at Thr^{18} increases the level of protection in the complexed ligand only. However, it should be emphasized that the fucosylation may actually also influence the exchange rate in free GFD, but this must then occur on a time scale that is too fast to be assessed by the present technique.

In contrast to the previously tested peptide ligands for uPAR, we do not observe any bimodal isotope distributions for GFD. In fact, there is no discernible broadening of the isotopic envelopes for the GFD modules, the widths of which remain essentially constant for even sustained periods of deuteration (up to 60 min) in the presence of uPAR. Concordantly, there is no evidence for the existence of correlated exchange of amide hydrogens, despite the fact that a substantial fraction of the GFD−uPAR complexes must have undergone dissociation during the 60 min of incubation (k_{off} for GFD−uPAR is 3.1×10^{-4} s^{-1} compared to 2.3×10^{-4} s^{-1} for AE105−uPAR as measured by surface plasmon resonance, see Table 1). The absence of peak broadening shows that dissociation of uPAR−GFD complexes is predominantly accompanied by an *uncorrelated* exchange. It is therefore impossible to calculate a dissociation *rate* constant for the GFD−uPAR complex by means of amide $^1H/^2H$ exchange and mass spectrometry, but it is should be emphasized that the *equilibrium* dissociation constant for this interaction can be derived using other established exchange methods (*27*, *28*).

The absence of correlated exchange for GFD strongly indicates that the amide hydrogens that become protected as a direct cause of the interaction with uPAR have exchange

[3] GFD_{1-45} contains only 42 main-chain amide hydrogens due to the presence of two proline residues. The deuterium loss as a result of acid quenching and desalting is thus (42−35)/42 ≈ 17%, which is comparable to that observed for the extended peptides AE133 and AE138: (13−11)/13 ≈ 15%. Completion of this exchange in GFD within 30 s at pD 8 is possible only with a lower limit of $k_{obs} > 0.2$ s^{-1}.

rates after dissociation that are substantially slower than their intrinsic chemical exchange rates. A significant stabilization of the GFD structure per se is probably induced by the interaction with uPAR. The observed protection levels are therefore most likely accounted for by a composite protection on some amide hydrogens that are directly engaged in the uPAR−GFD binding interface and on others that are involved in a receptor-induced reestablishment of the protein core in the GFD module. The short residence time of the free GFD ($t_R = 0.3$ s) is presumably the major rate-limiting step that abrogates detection of correlated exchange for even a subset of these amide hydrogens.

DISCUSSION

In the present study, we have analyzed the high-affinity interactions between the urokinase receptor (uPAR) and several small linear peptides as well as the GFD module of its cognate protein ligand (uPA) by amide $^1H/^2H$ exchange combined with mass spectrometry. Previously, it has been shown by amino acid replacements and surface plasmon resonance (*6*) that four of the side chains (Cha^2, Phe^3, Leu^7, and Trp^8) in the affinity optimized nine-mer peptide AE105 (Asp-**Cha**-**Phe**-ser-arg-Tyr-**Leu**-**Trp**-Ser) contribute significantly to the free energy of the interaction with uPAR and that the D-chirality of Ser^4 also adds to this high affinity ($K_d = 0.4$ nM). The present analysis of AE105 and its extended analogues by amide $^1H/^2H$ exchange clearly reveals an additional contribution from the majority of the main-chain amide hydrogens of AE105 to the interaction with uPAR, which implicates the involvement of at least six out of the eight main-chain amide hydrogens in this interaction. As deduced from studies on NH_2-terminally extended versions of AE105, the actual number of protected amide hydrogens is 7, which is further substantiated by data derived from additional $^2H/^1H$ exchange studies using predeuterated AE105 (data not shown). We find that the dissociation rates for the uPAR·AE105 complexes in solution, as measured by the correlated exchange, are in excellent agreement with those determined previously by surface plasmon resonance (*6*), further consolidating the specificity of both methods. Whether the slow-exchanging amide hydrogens of AE105 are engaged in an intermolecular hydrogen bonding network to uPAR, are shielded by the interface, or participate in self-contained intramolecular hydrogen bonds (e.g., in a β-hairpin or α-helix), or a combination of these cannot, however, be unraveled by the present technique. Nevertheless, the extensive engagement in hydrogen bonding on receptor binding emphasizes that this property must be taken into consideration when the transition of AE105 into smaller peptidomimetics is attempted by rational drug design.

The structural basis for the unusual protection of almost all amide hydrogens in AE105 on receptor binding remains to be clarified experimentally by NMR or X-ray crystallography. However, circumstantial evidence exists to suggest that the peptide antagonist is tightly imbedded between uPAR domains I and III, and this could consequently account for the high level of protection. Photoaffinity labeling of uPAR by a photoreactive precursor of AE105 thus led to the specific insertion into either Arg^{53} or Leu^{66} in loop 3 of uPAR domain I if Phe^3 in the peptide was replaced by benzophenone or (trifluoromethyl)-aryldiazirine (*10*, *11*). If, on the other hand, the photoreactive probe replaced Trp^8 in the peptide, the insertion occurred at His^{251} located in loop 3 of uPAR domain III (*10*, *11*). These observations subsequently led to the proposal that the peptide antagonist utilized a composite binding site assembled by interdomain interactions involving separate domains in the intact uPAR.

The other interaction that we have addressed in this study by amide $^1H/^2H$ exchange is the high-affinity binding between uPAR and the GFD module of the natural protease ligand, uPA. This module was the first EGF-like structure to be demonstrated to be modified by O-linked fucose (*16*), and it was subsequently reported that this modification is essential for an alleged growth promoting effect of uPA on the osteosarcoma cell-line SaOS-2 (*24*). An increasing number of EGF-like structures carrying a sequence-specific modification by O-linked fucose are now being recognized, and in specialized cases such as the membrane proteins Notch and Cripto, this carbohydrate is important for their ligand binding and signaling properties (*29*−*31*). Despite the fact that the fucosylation of the GFD of uPA does not have any major impact on the kinetics of the uPAR interaction per se, we nevertheless find that this fucose moiety does confer additional protein stability to the receptor-bound GFD as assessed by $^1H/^2H$ exchange experiments. Such stabilizing effect elicited by carbohydrate−polypeptide interactions is not a completely unprecedented phenomenon, since the presence of an O-linked fucose on Thr^9 in the small protease inhibitor PMP-C increases the thermal stability of the protein by approximately 1 kcal/mol and decreases the $^1H/^2H$ exchange rate for several backbone amide hydrogens located in the β-sheet (*32*). Although the fucose does not affect the kinetics of the primary interaction between uPAR and uPA, it may, however, modulate secondary interactions of the complex with other potential ligands such as vitronectin (*33*) and various integrins (*34*, *35*).

From a methodological point of view, this investigation also broadens the emerging vista in analyzing receptor−ligand interactions by amide hydrogen exchange combined with mass spectrometry. First, dissociation rate constants can be derived fairly accurately by this technique, as long as the recorded isotopic envelopes allow distinctions between correlated and uncorrelated exchange. Second, several structurally different ligands may be compared concomitantly under identical conditions in a single exchange experiment, as illustrated by the present analysis of receptor-bound GFD incompletely fucosylated on Thr^{18}. In this context, it will be very interesting to perform a careful analysis of the exchange properties of a trimolecular complex that is formed between uPAR, uPA, and the small somatomedin B domain of vitronectin (*33*). Finally, the uPAR-induced selectivity and polarization in the deuteron distribution of the extended versions of AE105 may provide the necessary experimental tools to settle the persisting controversy in the literature regarding the occurrence of collision-induced scrambling of amide hydrogens during MS-MS sequencing (*36*, *37*).

ACKNOWLEDGMENT

The authors thank Yvonne DeLotto, Gitte Juhl Funch, and John Post for excellent technical assistance. The critical comments on the manuscript by Drs. Vincent Ellis (University of East Anglia, U.K.) and Geoffrey M. Kellerman (Hunter Area Pathology Service, Newcastle, Australia) are greatly appreciated.

REFERENCES

1. Clackson, T., and Wells, J. A. (1995) A hot spot of binding energy in a hormone-receptor interface, *Science 267*, 383−386.
2. Burnens, A., Demotz, S., Corradin, G., Binz, H., and Bosshard, H. R. (1987) Epitope mapping by chemical modification of free and antibody-bound protein antigen, *Science 235*, 780−783.
3. Ploug, M., Rahbek-Nielsen, H., Ellis, V., Roepstorff, P., and Danø, K. (1995) Chemical modification of the urokinase-type plasminogen activator and its receptor using tetranitromethane. Evidence for the involvement of specific tyrosine residues in both molecules during receptor−ligand interaction, *Biochemistry 34*, 12524−12534.
4. Mandell, J. G., Falick, A. M., and Komives, E. A. (1998) Identification of protein−protein interfaces by decreased amide proton solvent accessibility, *Proc. Natl. Acad. Sci. U.S.A. 95*, 14705−14710.
5. Arrington, C. B., Teesch, L. M., and Robertson, A. D. (1999) Defining protein ensembles with native-state NH exchange: kinetics of interconversion and cooperative units from combined NMR and MS analysis, *J. Mol. Biol. 285*, 1265−1275.
6. Ploug, M., Østergaard, S., Gårdsvoll, H., Kovalski, K., Holst-Hansen, C., Holm, A., Ossowski, L., and Danø, K. (2001) Peptide-derived antagonists of the urokinase receptor. affinity maturation by combinatorial chemistry, identification of functional epitopes, and inhibitory effect on cancer cell intravasation, *Biochemistry 40*, 12157−12168.
7. Ploug, M., Rønne, E., Behrendt, N., Jensen, A. L., Blasi, F., and Danø, K. (1991) Cellular receptor for urokinase plasminogen activator. Carboxyl-terminal processing and membrane anchoring by glycosyl-phosphatidylinositol, *J. Biol. Chem. 266*, 1926−1933.
8. Ellis, V. (2003) Plasminogen activation at the cell surface, *Curr. Top. Dev. Biol. 54*, 263−312.
9. Ploug, M. (2003) Structure−function relationships in the interaction between the urokinase-type plasminogen activator and its receptor, *Curr. Pharm. Des. 9*, 639−652.
10. Ploug, M., Østergaard, S., Hansen, L. B., Holm, A., and Danø, K. (1998) Photoaffinity labeling of the human receptor for urokinase-type plasminogen activator using a decapeptide antagonist. Evidence for a composite ligand-binding site and a short interdomain separation, *Biochemistry 37*, 3612−3622.
11. Ploug, M. (1998) Identification of specific sites involved in ligand binding by photoaffinity labeling of the receptor for the urokinase-type plasminogen activator. Residues located at equivalent positions in uPAR domains I and III participate in the assembly of a composite ligand-binding site, *Biochemistry 37*, 16494−16505.
12. Gårdsvoll, H., Danø, K., and Ploug, M. (1999) Mapping part of the functional epitope for ligand binding on the receptor for urokinase-type plasminogen activator by site-directed mutagenesis, *J. Biol. Chem. 274*, 37995−38003.
13. Ploug, M., Rahbek-Nielsen, H., Nielsen, P. F., Roepstorff, P., and Danø, K. (1998) Glycosylation profile of a recombinant urokinase-type plasminogen activator receptor expressed in Chinese hamster ovary cells, *J. Biol. Chem. 273*, 13933−13943.
14. Bugge, T. H., Lund, L. R., Kombrinck, K. K., Nielsen, B. S., Holmback, K., Drew, A. F., Flick, M. J., Witte, D. P., Danø, K., and Degen, J. L. (1998) Reduced metastasis of Polyoma virus middle T antigen-induced mammary cancer in plasminogen-deficient mice, *Oncogene 16*, 3097−3104.
15. Rømer, J., Nielsen, B. S., and Ploug, M. (2004) The urokinase receptor as a potential target in cancer therapy, *Curr. Pharm. Des. 10*, 2359−2376.
16. Buko, A. M., Kentzer, E. J., Petros, A., Menon, G., Zuiderweg, E. R., and Sarin, V. K. (1991) Characterization of a posttranslational fucosylation in the growth factor domain of urinary plasminogen activator, *Proc. Natl. Acad. Sci. U.S.A. 88*, 3992−3996.
17. Bai, Y., Milne, J. S., Mayne, L., and Englander, S. W. (1993) Primary structure effects on peptide group hydrogen exchange, *Proteins 17*, 75−86.
18. Milne, J. S., Mayne, L., Roder, H., Wand, A. J., and Englander, S. W. (1998) Determinants of protein hydrogen exchange studied in equine cytochrome *c*, *Protein Sci. 7*, 739−745.
19. Yi, Q., and Baker, D. (1996) Direct evidence for a two-state protein unfolding transition from hydrogen−deuterium exchange, mass spectrometry, and NMR, *Protein Sci. 5*, 1060−1066.
20. Miranker, A., Robinson, C. V., Radford, S. E., Aplin, R. T., and Dobson, C. M. (1993) Detection of transient protein folding populations by mass spectrometry, *Science 262*, 896−900.
21. Arrington, C. B., and Robertson, A. D. (2000) Correlated motions in native proteins from MS analysis of NH exchange: evidence for a manifold of unfolding reactions in ovomucoid third domain, *J. Mol. Biol. 300*, 221−232.
22. Harris, D. C. (1998) Nonlinear least-squares curve fitting with Microsoft excel solver, *J. Chem. Educ. 75*, 119−121.
23. Magdolen, V., Rettenberger, P., Koppitz, M., Goretzki, L., Kessler, H., Weidle, U. H., Konig, B., Graeff, H., Schmitt, M., and Wilhelm, O. (1996) Systematic mutational analysis of the receptor-binding region of the human urokinase-type plasminogen activator, *Eur. J. Biochem. 237*, 743−751.
24. Rabbani, S. A., Mazar, A. P., Bernier, S. M., Haq, M., Bolivar, I., Henkin, J., and Goltzman, D. (1992) Structural requirements for the growth factor activity of the amino-terminal domain of urokinase, *J. Biol. Chem. 267*, 14151−14156.
25. Rabbani, S. A., Desjardins, J., Bell, A. W., Banville, D., Mazar, A., Henkin, J., and Goltzman, D. (1990) An amino-terminal fragment of urokinase isolated from a prostate cancer cell line (PC-3) is mitogenic for osteoblast-like cells, *Biochem. Biophys. Res. Commun. 173*, 1058−1064.
26. Hansen, A. P., Petros, A. M., Meadows, R. P., Nettesheim, D. G., Mazar, A. P., Olejniczak, E. T., Xu, R. X., Pederson, T. M., Henkin, J., and Fesik, S. W. (1994) Solution structure of the amino-terminal fragment of urokinase-type plasminogen activator, *Biochemistry 33*, 4847−4864.
27. Powell, K. D., Ghaemmaghami, S., Wang, M. Z., Ma, L. Y., Oas, T. G., and Fitzgerald, M. C. (2002) A general mass spectrometry-based assay for the quantitation of protein−ligand binding interactions in solution, *J. Am. Chem. Soc. 124*, 10256−10257.
28. Zhu, M. M., Rempel, D. L., Du, Z. H., and Gross, M. L. (2003) Quantification of protein−ligand interactions by mass spectrometry, titration, and H/D exchange: PLIMSTEX, *J. Am. Chem. Soc. 125*, 5252−5253.
29. Schiffer, S. G., Foley, S., Kaffashan, A., Hronowski, X., Zichittella, A. E., Yeo, C. Y., Miatkowski, K., Adkins, H. B., Damon, B., Whitman, M., Salomon, D., Sanicola, M., and Williams, K. P. (2001) Fucosylation of Cripto is required for its ability to facilitate nodal signaling, *J. Biol. Chem. 276*, 37769−37778.
30. Okajima, T., Xu, A., and Irvine, K. D. (2003) Modulation of notch-ligand binding by protein O-fucosyltransferase 1 and fringe, *J. Biol. Chem. 278*, 42340−42345.
31. Okajima, T., and Irvine, K. D. (2002) Regulation of notch signaling by o-linked fucose, *Cell 111*, 893−904.
32. Mer, G., Hietter, H., and Lefevre, J. F. (1996) Stabilization of proteins by glycosylation examined by NMR analysis of a fucosylated proteinase inhibitor, *Nat. Struct. Biol. 3*, 45−53.
33. Deng, G., Curriden, S. A., Wang, S., Rosenberg, S., and Loskutoff, D. J. (1996) Is plasminogen activator inhibitor-1 the molecular switch that governs urokinase receptor-mediated cell adhesion and release? *J. Cell. Biol. 134*, 1563−1571.
34. Wei, Y., Lukashev, M., Simon, D. I., Bodary, S. C., Rosenberg, S., Doyle, M. V., and Chapman, H. A. (1996) Regulation of integrin function by the urokinase receptor, *Science 273*, 1551−1555.
35. Pluskota, E., Soloviev, D. A., and Plow, E. F. (2003) Convergence of the adhesive and fibrinolytic systems: recognition of urokinase by integrin alpha Mbeta 2 as well as by the urokinase receptor regulates cell adhesion and migration, *Blood 101*, 1582−1590.
36. Demmers, J. A., Rijkers, D. T., Haverkamp, J., Killian, J. A., and Heck, A. J. (2002) Factors affecting gas-phase deuterium scrambling in peptide ions and their implications for protein structure determination, *J. Am. Chem. Soc. 124*, 11191−11198.
37. Deng, Y., Pan, H., and Smith, D. L. (1999) Selective isotope labeling demonstrates that hydrogen exchange at individual peptide amide linkages can be determined by collision-induced dissociation mass spectrometry, *J. Am. Chem. Soc. 121*, 1966−1967.
38. Zhang, Z., and Smith, D. L. (1993) Determination of amide hydrogen exchange by mass spectrometry: a new tool for protein structure elucidation, *Protein Sci. 2*, 522−531.

BI048706J